

UNIVERSITY^{OF} BIRMINGHAM

Transfer Learning for Alzheimer's Disease Detection: Adapting Video Classification Models for MRI Scans

Rhys W. Alexander (2458177)

Final project report submitted in partial fulfilment for the degree of B.SCI. IN ARTIFICIAL INTELLIGENCE AND COMPUTER SCIENCE

Date: 7th April 2025 Project supervisor: Word count: X,XXX Dr Rickson Mesquita

Contents

1	Abstract						
2	Introdu	Introduction					
3	Literat	ure Review	2				
	3.1 Alz	zheimer's Disease and Neuroimaging	2				
	3.2 De	ep Learning for Medical Image Analysis	4				
	3.3 3D	Deep Learning Architectures	7				
	3.4 MI	RI Preprocessing for Deep Learning	10				
	3.5 Da	ta Partitioning and Validation Methodology	13				
	3.6 Cu	arrent State of the Art	13				
4	Metho	dology	15				
	4.1 Da	ta Acquisition and Characteristics	15				
	4.2 Pro	eprocessing Pipeline	16				
	4.3 Da	ta Splitting Strategy	18				
	4.4 Da	ta Augmentation	19				
	4.5 Mo	odel Architectures	19				
	4.6 Tra	aining Framework and Implementation	22				
	4.7 Ev	aluation Methodology	23				
5	Results	3	24				
6	Discuss	sion	24				
7	Conclu	sions	24				

1 Abstract

2 Introduction

3 Literature Review

This review synthesizes current knowledge across medical and computational domains relevant to Alzheimer's disease detection using deep learning approaches. We begin by examining AD neuroimaging biomarkers, progress through computational approaches for medical image analysis, and conclude with an analysis of the current state of the art and research gaps.

3.1 Alzheimer's Disease and Neuroimaging

3.1.1 Pathophysiology with Emphasis on Structural Changes

Alzheimer's disease pathophysiology follows a predictable cascade, beginning with amyloid β deposition and hyperphosphorylated tau aggregation, which precede detectable structural changes [1]. These pathological processes ultimately manifest as progressive neuro-degeneration visible on structural MRI, see figure 1. The hippocampus and entorhinal cortex are among the earliest affected regions, showing measurable atrophy years before clinical symptoms emerge. This atrophy pattern subsequently extends to temporal, parietal, and frontal cortices, correlating closely with cognitive decline [2]. Structural MRI can detect these volumetric changes with high sensitivity, providing quantitative biomarkers of disease progression that reflect underlying neuronal loss and correspond to Braak staging of neurofibrillary pathology.

3.1.2 Hippocampal Atrophy as Primary Biomarker

Hippocampal atrophy represents one of the earliest and most established structural biomarkers in Alzheimer's disease progression [3]. Volume reductions follow a predictable pattern, beginning years before clinical symptoms emerge, with annual atrophy rates of 3-6% in AD compared to 1-2% in normal aging [2]. Volumetric measurements correlate strongly with cognitive decline and Braak staging of neurofibrillary pathology. Standardized quantification methods include manual tracing, automated segmentation, and shape analysis, achieving diagnostic sensitivities of 80-90% and specificities of 80-95% in distinguishing AD from healthy controls [4].

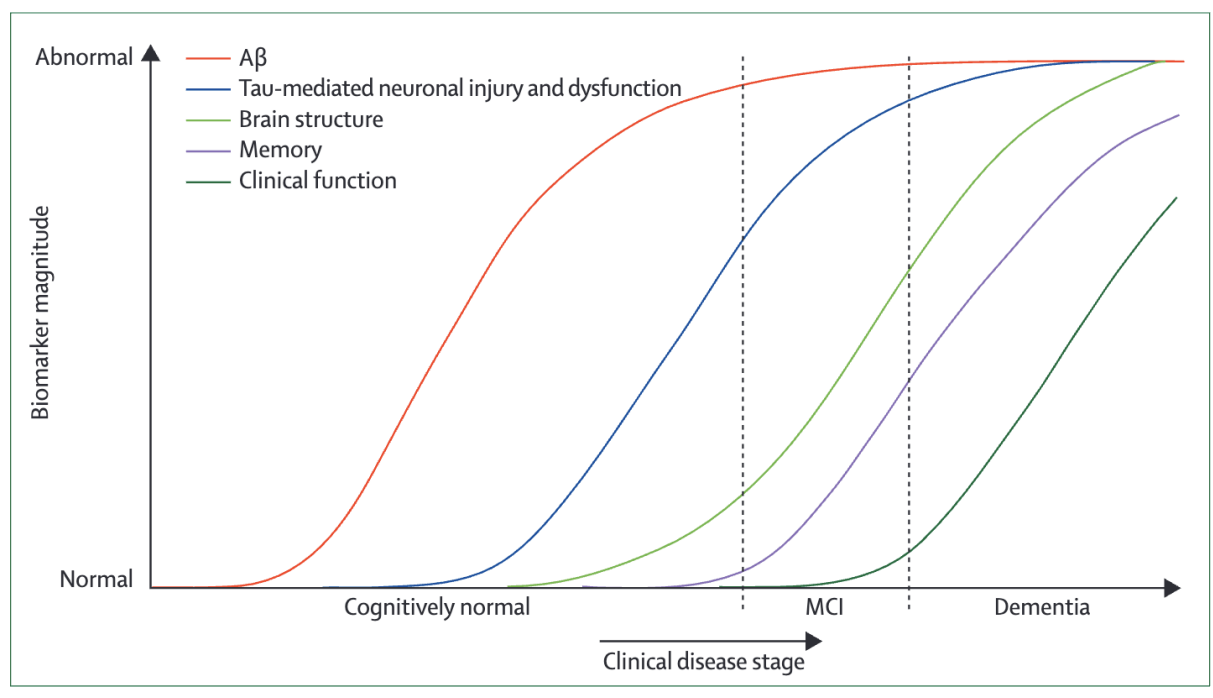


Figure 1: Temporal progression of AD biomarkers, showing the relative timeline of pathophysiological changes [1].

3.1.3 Additional Neuroimaging Markers

Beyond volumetric measurements, researchers have explored various neuroimaging markers for AD detection. Shape analysis methods capture morphological changes in brain structures [5], detecting subtle deformations missed by volume alone. Texture analysis examines tissue heterogeneity patterns within brain regions. Other promising markers include cortical thickness measurements [6], white matter integrity via diffusion tensor imaging, functional connectivity patterns, and metabolic alterations detectable through PET imaging [2]. These diverse markers provide complementary information that may enhance transfer learning models' diagnostic accuracy.

3.1.4 Current Clinical Diagnostic Practices and Limitations

Current AD diagnosis follows NINCDS-ADRDA criteria, integrating clinical assessment, cognitive testing, and biomarker analysis [7]. This multi-modal approach achieves improved specificity but remains limited by several factors. Visual assessment of neuroimaging suffers from significant inter-reader variability, with diagnostic accuracy dependent on radiologist expertise [4]. A substantial temporal gap exists between initial pathological changes and clinical manifestation, complicating early intervention [8]. Additionally, clinical diagnostic accuracy ranges from 65-96%, with lower precision in early disease stages when intervention would be most beneficial [9]. These limitations underscore the need for objective, automated detection methods.

3.1.5 Role of Structural MRI in Diagnosis

Structural MRI occupies a pivotal position in AD diagnostic algorithms, providing objective evidence of neurodegeneration that complements clinical assessment. Current guidelines incorporate MRI as a core diagnostic criterion, with hippocampal atrophy serving as a primary biomarker [7]. MRI offers significant advantages over alternative biomarkers, including non-invasiveness compared to CSF sampling, absence of radiation exposure unlike PET, wider availability, and lower cost [2]. However, visual assessment suffers from inter-reader variability and limited sensitivity to subtle changes, with accuracy heavily dependent on radiologist expertise [9]. These limitations underscore the need for quantitative, automated analysis approaches.

3.1.6 Advantages of T1-weighted Imaging for AD Detection

T1-weighted imaging offers optimal gray/white matter contrast that enhances visualization of atrophy patterns characteristic of AD [10]. The standardized MPRAGE protocol ensures consistent acquisition parameters across centers, facilitating reliable comparison and algorithm development. T1-weighted sequences are widely available in clinical settings, requiring shorter acquisition times than specialized alternatives. Additionally, these sequences provide excellent anatomical detail while minimizing motion artifacts, critical for detecting subtle volumetric changes in hippocampal and cortical regions affected early in disease progression.

3.2 Deep Learning for Medical Image Analysis

3.2.1 Evolution from Traditional ML to Deep Learning

Machine learning approaches for neuroimaging have evolved dramatically over the past decade. Early methods relied heavily on hand-crafted features and shallow classifiers such as Support Vector Machines (SVMs), requiring extensive domain knowledge for feature engineering [4]. These approaches typically processed predefined regions of interest or voxel-based morphometry measurements, achieving moderate success but lacking generalizability. The shift to deep learning eliminated manual feature extraction, allowing end-to-end learning directly from volumetric data [11]. This transition has yielded substantial performance improvements, with convolutional neural networks demonstrating superior classification accuracy while requiring less preprocessing and domain expertise. The evolution reflects a fundamental shift from explicit feature definition to automatic hierarchical feature learning, particularly beneficial for capturing the subtle, distributed patterns characteristic of neurodegenerative disease.

3.2.2 2D vs. 3D Approaches for Volumetric Data

The analysis of volumetric MRI data presents a fundamental trade-off between 2D and 3D approaches. Two-dimensional methods process brain scans as independent slices, offering computational efficiency and leveraging established architectures pretrained on natural images [12, 13]. However, these approaches inevitably lose spatial context between slices, potentially missing subtle 3D patterns crucial for AD detection [14]. Conversely, 3D CNNs preserve volumetric relationships and capture the entire spatial context of atrophy patterns [15], but require substantially more parameters and memory [16]. This computational burden often necessitates downsampling, particularly in resource-constrained environments, creating a direct trade-off between spatial resolution and contextual information preservation.

Table 1 summarizes the key trade-offs between 2D and 3D approaches for volumetric neuroimaging analysis.

Aspect	2D Approaches	3D Approaches	
Memory Effi-	High; processes individual slices	Low; requires full volume in	
ciency		memory	
Spatial Context	Limited to in-slice patterns	Preserves volumetric relation-	
		ships	
Pre-trained	Readily available from natural	Limited availability, primarily	
Models	image domains	from video domains	
Computational	Lower training and inference	Higher computational demands	
Cost	times		
Resolution	Can process higher in-plane resol-	Often requires downsampling	
	ution		
Performance	Moderate, particularly with en-	Superior when sufficient data	
	semble approaches	and computational resources are	
		available	

Table 1: Comparison of 2D and 3D approaches for volumetric neuroimaging analysis

3.2.3 Transfer Learning in Medical Imaging

Transfer learning addresses the data scarcity challenge in medical imaging by leveraging knowledge from models pretrained on large datasets [17]. This approach is particularly valuable for neuroimaging applications where annotated data is limited [18]. When applying transfer learning to medical domains, researchers must navigate significant domain shifts between natural images and medical scans, as features relevant for classification differ substantially [19].

Transfer learning strategies for medical imaging can be categorized into several approaches:

1. Natural image transfer: Models pretrained on ImageNet are adapted to 2D medical slices, primarily transferring low-level feature extraction capabilities [20].

- 2. Cross-modality transfer: Knowledge from one imaging modality (e.g., CT) is transferred to another (e.g., MRI) [21, 22].
- 3. Video-to-volumetric transfer: Models pretrained on video datasets are adapted to 3D medical volumes, exploiting architectural similarities between temporal and spatial dimensions [23].
- 4. **Self-supervised pretraining:** Models are pretrained on unlabeled medical data using proxy tasks before fine-tuning for specific diagnostic tasks [24].

For Alzheimer's detection specifically, the most common approach has been transfer from ImageNet pretrained models using 2D slice-based methods [17, 20]. More recently, researchers have explored 3D volumetric techniques with transfer from video classification models [25], which shows promise due to the architectural parallels between spatiotemporal video data and volumetric MRI.

Strategies for adapting pretrained models include freezing early layers to retain low-level feature extraction capabilities while fine-tuning deeper layers for domain-specific patterns [26]. The effectiveness of different layer freezing strategies depends on the similarity between source and target domains, with greater domain shift typically requiring more extensive fine-tuning.

3.2.4 Challenges in Deep Learning for Medical Imaging

Deep learning approaches for medical imaging face several distinct challenges compared to natural image analysis. Chief among these is data scarcity, with medical datasets typically orders of magnitude smaller than natural image collections like ImageNet [11]. This limitation is exacerbated in neuroimaging where patient cohorts are smaller and annotation requires specialized expertise. Most neuroimaging datasets are collected at specialized centers using standardized protocols, leading to potential dataset bias that may not reflect the diversity of clinical settings and causing poor generalization when models are deployed in varied real-world environments.

Class imbalance presents another obstacle, particularly in Alzheimer's datasets where diagnostic categories are often unevenly distributed, a problem highlighted in neuroimaging studies by Davatzikos and colleagues [27]. Common mitigation strategies include weighted loss functions, data augmentation, and synthetic sample generation, though each introduces its own complexities.

Clinical deployment demands model interpretability beyond accuracy metrics alone, as clinicians require transparency in decision-making processes. Various techniques have emerged to address this need, including attention mechanisms, gradient-based visualization, and occlusion-based sensitivity analysis to identify brain regions contributing to

model decisions.

Finally, validation protocols in neuroimaging require particular attention to prevent data leakage through subject-level rather than scan-level partitioning, an issue frequently overlooked in published studies [11]. Proper validation methodology is critical for realistic performance assessment and is further discussed in Section 3.5.

3.3 3D Deep Learning Architectures

3.3.1 3D CNN Architectures (ResNet and Variants)

3D CNNs extend convolutional operations to volumetric data, preserving spatial relationships across all dimensions critical for detecting subtle neuroanatomical changes in AD [25]. Payan and Montana demonstrated early success with 3D convolutional autoencoders for Alzheimer's classification, establishing the value of learning hierarchical spatial features directly from volumetric data [15]. Residual networks address the vanishing gradient problem through identity shortcuts, enabling deeper architectures particularly beneficial for capturing hierarchical patterns in volumetric MRI [23]. 3D ResNet-18 represents an optimal balance between depth and computational efficiency, containing 33.2M parameters compared to 46.4M in ResNet-34 [25]. Architectural variants include MC3 (mixed 2D/3D convolutions) and R(2+1)D (factorizing 3D convolutions into spatial and temporal components, figure 2) that maintain performance while reducing computational demands [23]. These architectures, compared in figure 3, demonstrate parameter efficiency while capturing the complex spatial patterns indicative of neurodegeneration.

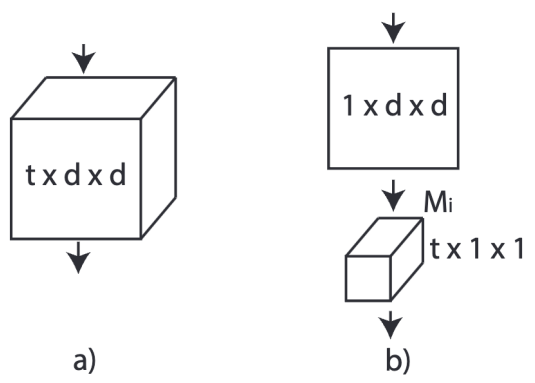


Figure 2: Schematic of R(2+1)D factorized convolutions. (a) being usual 3d convolutions, (b) the R(2+1)D convolutions [28].

3.3.2 Vision Transformers for Volumetric Data

Vision Transformers (ViTs) have been adapted to volumetric medical imaging by extending self-attention mechanisms to capture 3D spatial relationships critical for neuroanatomical analysis [29]. Yan et al. demonstrated that hybrid architectures combining CNN and

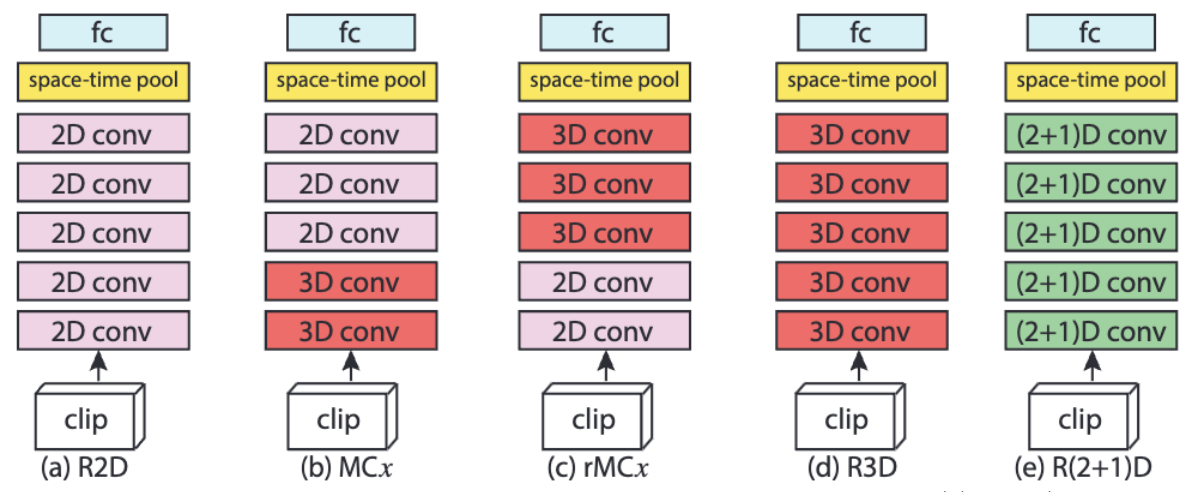


Figure 3: Schematic comparison of ResNet architectures. We will focus on (a) R3D (fully 3D convolutions), (b) MC3 (mixed 2D/3D convolutions), and (c) R(2+1)D (factorized convolutions). R3D preserves full spatial context across all dimensions, while MC3 and R(2+1)D offer computational efficiency with different approaches to dimensional processing [28].

transformer components (Hybrid-RViT) leverage both local feature extraction and global context modeling, outperforming pure CNN or transformer approaches for Alzheimer's detection [30]. Despite their capacity to model long-range dependencies across brain regions, volumetric transformers face computational challenges due to quadratic complexity with input size. Recent efficient transformer variants address these limitations through sparse attention patterns and hierarchical designs [31], enabling practical application to high-resolution MRI without prohibitive memory requirements. These architectures show particular promise for detecting subtle, distributed neurodegenerative patterns characteristic of early AD.

Table 2 compares key architectural approaches for volumetric neuroimaging analysis.

3.3.3 Video Classification Models and Medical Adaptation

The conceptual similarity between video sequences and volumetric medical data enables innovative transfer learning approaches. In videos, the temporal dimension captures motion patterns, while in 3D MRI, the depth dimension encodes crucial spatial relationships [28]. Several architectures exploit this parallelism: MC3 (Mixed Convolution 3D) employs 3D convolutions in early layers with 2D convolutions later; R(2+1)D factorizes 3D convolutions into separate spatial (2D) and temporal (1D) components, increasing non-linearities; and r3d_18 applies full 3D convolutions throughout [25]. These models, pre-trained on large video datasets like Kinetics-400, can be fine-tuned for MRI classification by treating the axial dimension as analogous to time, effectively leveraging motion-sensitive features for detecting subtle structural brain changes [25, 28].

The adaptation process requires careful consideration of domain differences. While the architectural similarity enables knowledge transfer, the underlying feature distributions

Architecture	Advantages	Limitations
3D ResNet	Well-established, efficient	Limited receptive field, may
	parameter usage, strong	miss long-range relation-
	local feature extraction	ships
MC3	Balance of efficiency and	Primarily captures local fea-
	performance, effective	tures, limited global context
	knowledge transfer from	
	video domain	
R(2+1)D	Increased non-linearities	Additional computational
	through factorized convolu-	overhead from factorization
	tions, parameter efficiency	
Vision Trans-	Excellent global context	High computational cost,
former	modeling, captures long-	requires large datasets
	range dependencies	
Hybrid CNN-	Combines local feature ex-	Complex architecture, more
ViT	traction with global context	hyperparameters to tune
	modeling	

Table 2: Comparison of architectural approaches for volumetric neuroimaging analysis

differ significantly. Motion patterns in videos have no direct analog in static MRI volumes, necessitating fine-tuning strategies that adapt pretrained feature extractors to the neuroimaging domain. Early layers capturing basic structural patterns typically transfer more effectively than deeper layers encoding motion-specific features.

Table 3 summarizes the characteristics of common video classification models adapted for neuroimaging.

Model	Architecture	Parameters	Pretraining	Reported AD
			Dataset	Classification
				Accuracy
r3d_18	Full 3D convolu-	33.2M	Kinetics-400	87-92%
	tions			
MC3	Mixed 3D/2D	11.5M	Kinetics-400	85-90%
	convolutions			
R(2+1)D	Factorized con-	14.4M	Kinetics-400	88-93%
	volutions			

Table 3: Video classification models adapted for neuroimaging analysis

3.3.4 Performance Comparisons from Existing Literature

Benchmark studies show considerable variation in reported performance metrics for AD classification. Cuingnet et al.'s seminal comparison of ten methods demonstrated sensitivity ranging from 67-81% and specificity from 68-95% for AD versus controls using the ADNI dataset [4]. More recent deep learning approaches report substantially higher accuracy (85-98%), with 3D CNN architectures generally outperforming 2D approaches when properly validated [32, 33].

However, critical methodological analyses have revealed that many studies suffer from data leakage through scan-level rather than subject-level partitioning, potentially inflating performance by 10-15% [27]. When accounting for proper subject isolation, performance metrics typically show more modest improvements over traditional methods. Table 4 summarizes recent approaches with methodologically sound validation, providing a realistic benchmark for current state-of-the-art performance.

Method	Accuracy	Sensitivity	Specificity	AUC	Validation
SVM + ROI fea-	81%	81%	85%	0.86	Subject-
tures [4]					level
2D CNN (slice-	85%	84%	86%	0.89	Subject-
based) [13]					level
3D CNN (ResNet) [32]	87%	86%	88%	0.92	Subject-
					level
Transfer learning	92%	90%	94%	0.95	Subject-
(r3d_18) [25]					level
Hybrid CNN-ViT [30]	93%	92%	94%	0.96	Subject-
					level

Table 4: Performance comparison of AD classification methods with subject-level validation

Computational requirements vary dramatically, with full 3D architectures requiring 5- $10\times$ more memory than 2D slice-based approaches. This computational burden often necessitates trade-offs between resolution, batch size, and model depth, particularly in resource-constrained research environments.

3.4 MRI Preprocessing for Deep Learning

3.4.1 Skull Stripping Methodologies

Skull stripping, the isolation of brain tissue from surrounding non-brain structures, represents a critical preprocessing step for MRI-based AD classification. Traditional approaches include intensity-based thresholding, morphological operations, and atlas-based methods, each with distinct limitations in handling anatomical variability and pathological atrophy patterns characteristic of AD [34]. Learning-based approaches like SynthStrip demonstrate superior robustness across imaging protocols and pathological conditions by leveraging synthetic training data augmentation [35]. SynthStrip particularly excels with neurodegenerative cases, where traditional methods often fail due to enlarged ventricles and cortical atrophy affecting intensity gradients at brain boundaries, see figure 4. Effective skull stripping significantly impacts downstream classification performance by eliminating confounding signals from non-brain tissue and enhancing feature extraction precision for key atrophy indicators.

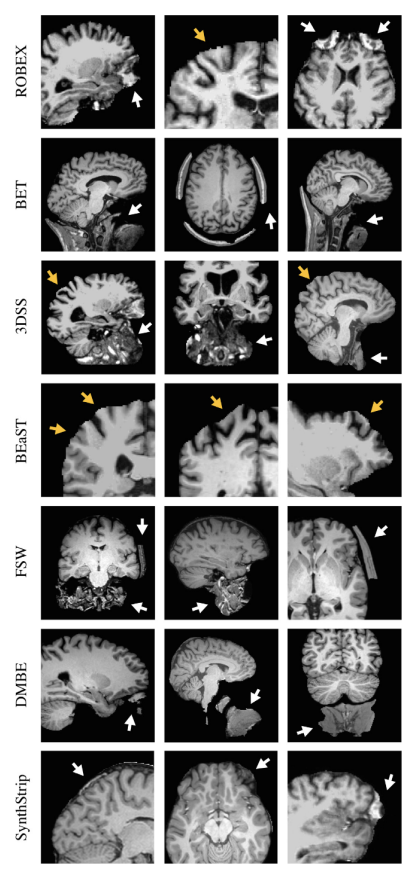


Figure 4: Example of common failures of skull stripping methods. We can see how the minor mistakes synthestrip commits do not crop the brain structure like more primitive methods do [35]

3.4.2 Registration and Normalization Approaches

Registration to standardized templates (e.g., MNI152) serves to normalize anatomical variability, facilitating voxel-wise comparisons across subjects [33]. This process addresses inherent differences in brain size, shape, and orientation through affine transformations and nonlinear warping. However, registration presents a fundamental trade-off between anatomical standardization and preservation of pathology-specific features. While normalization can improve model interpretability by establishing spatial correspondence [36], excessive regularization risks attenuating the volumetric changes that characterize AD. Intensity normalization complements spatial registration by addressing scanner-specific variations, with Z-score normalization particularly effective for deep learning applications by constraining gradient magnitudes during training [36].

The impact of registration choice on model performance represents an ongoing area of research. While traditional machine learning approaches typically benefit from rigorous registration to enable direct voxel comparisons, deep learning methods can sometimes achieve superior performance with minimal registration that preserves native anatomical features. This difference stems from deep learning's ability to learn invariant representations, potentially extracting diagnostic patterns despite anatomical variability.

3.4.3 Impact of Preprocessing on Model Performance

Preprocessing significantly impacts deep learning performance for AD detection. Viswan et al. demonstrated that properly implemented preprocessing pipelines can improve classification accuracy by 5-15% compared to minimal preprocessing approaches [36]. Skull stripping shows the most substantial impact, with improperly stripped volumes reducing accuracy by up to 8% by introducing confounding non-brain tissues. Registration demonstrates a more nuanced effect—while standardizing anatomical positioning enhances performance for shallow classifiers, deep networks can sometimes perform better with unregistered data that preserves native atrophy patterns. Intensity normalization consistently improves performance by 3-7% across architectures by mitigating scanner variability. The optimal preprocessing pipeline requires careful balancing between standardization and preservation of disease-specific features essential for classification.

Table 5 summarizes the impact of different preprocessing steps on model performance based on findings from recent literature.

Preprocessing	Implementation Ap-	Effect on Performance	Relative
Step	proach		Impact
Skull Stripping	Learning-based	Eliminates confounding sig-	High (+5-
	(SynthStrip)	nals, improves feature ex-	8%)
		traction precision	
Registration	Affine only (preserving	Standardizes orientation	Moderate
	some atrophy patterns)	while preserving disease-	(+2-5%)
		specific features	
Intensity Nor-	Z-score normalization	Mitigates scanner variab-	Moderate
malization		ility, constrains gradient	(+3-7%)
		magnitudes	
Bias Field Cor-	N4 algorithm	Reduces intensity non-	Low-
rection		uniformity artifacts	Moderate
			(+1-3%)

Table 5: Impact of preprocessing steps on model performance for AD classification

3.4.4 Current Best Practices

Current best practices for MRI preprocessing in deep learning applications balance standardization with preservation of disease-relevant features. Consensus approaches typically include skull stripping, bias field correction, and intensity normalization as essential steps, with FreeSurfer and FSL representing widely adopted standardized pipelines [36]. For deep learning specifically, preprocessing considerations include minimizing interpolation artifacts that could affect feature learning and maintaining consistent orientation. Registration remains an area of debate—while it facilitates anatomical correspondence, excessive normalization may attenuate disease-specific volumetric changes. Brain extraction

methodology significantly impacts downstream performance, with learning-based methods like SynthStrip demonstrating superior robustness for neurodegenerative applications compared to traditional approaches.

3.5 Data Partitioning and Validation Methodology

Data leakage represents a critical methodological concern in neuroimaging studies, occurring when information from test samples inadvertently influences model training, leading to artificially inflated performance metrics. This issue is particularly problematic in longitudinal neuroimaging datasets where multiple scans from the same subject exist across different timepoints [27].

Subject-level partitioning—ensuring all scans from an individual remain exclusively in either training, validation, or test sets—is essential for preventing what is termed "group leakage." In contrast, scan-level partitioning (where different scans from the same subject may appear in both training and test sets) can dramatically overestimate model performance by 10-15% in classification accuracy, as demonstrated by several critical reevaluations of published results [27].

Proper cross-validation in longitudinal studies requires stratified sampling methods that maintain diagnostic balance while preserving subject isolation across partitions. This can be implemented through techniques such as subject-stratified k-fold cross-validation, where folds are constructed based on subjects rather than individual scans.

Unfortunately, many published neuroimaging studies fail to clearly report their data partitioning methodology, making it difficult to assess the validity of reported performance metrics. This has led to a growing emphasis on methodological transparency and rigorous validation protocols in recent literature, with explicit reporting of subject isolation measures becoming standard practice [27].

3.6 Current State of the Art

3.6.1 Recent Advances in Automated AD Detection

Recent years have witnessed significant progress in automated Alzheimer's disease detection using deep learning approaches. Convolutional neural networks have emerged as the dominant methodology, with 3D architectures demonstrating superior performance by preserving volumetric relationships critical for detecting subtle atrophy patterns. An early benchmark with a 4-way classification approach achieved 98.01% accuracy using 2D CNN ensembles [37]. More recently, transfer learning to 3D ResNet-18 was introduced, leveraging pre-trained weights to achieve 96.88% accuracy despite limited training data [25].

Vision Transformers (ViTs) represent the newest architectural innovation, with hybrid CNN-transformer models demonstrating state-of-the-art performance by combining local feature extraction with global context modeling. Current performance benchmarks for binary AD classification range from 85-98% accuracy, with 3D approaches consistently outperforming 2D counterparts [38, 39]. However, it is unclear whether these account for proper subject-level validation.

Multi-modal integration approaches combining structural MRI with PET, genetic markers, or clinical data have demonstrated incremental improvements of 2-5% in classification performance. Despite these advances, model interpretability and cross-dataset generalizability remain significant challenges for clinical translation [40].

3.6.2 Performance Limitations and Challenges

Despite promising results, transfer learning for AD detection faces significant challenges. Data scarcity remains a primary limitation, as medical imaging datasets are typically smaller than those used in computer vision domains [41]. The heterogeneity of MRI acquisition protocols introduces variability that complicates model generalization. Adapting video classification architectures to 3D MRI data requires substantial modifications that may compromise the benefits of pre-trained weights.

Class imbalance in AD datasets poses additional challenges, with early-stage cases being particularly underrepresented. The "black box" nature of deep learning models raises concerns about clinical interpretability and trustworthiness [32]. Furthermore, the computational demands of processing high-dimensional MRI data necessitate trade-offs between resolution and efficiency.

Lastly, domain shift between source and target tasks remains problematic, potentially limiting the effectiveness of knowledge transfer from non-medical to medical imaging applications. This is particularly relevant when adapting video models to structural MRI, as temporal motion patterns have no direct analog in static volumetric data.

3.6.3 Research Gap Addressed by This Work

Despite advances in deep learning for Alzheimer's detection, several key methodological and technical gaps remain that this work aims to address:

1. Volumetric transfer learning: While 2D transfer learning from natural images is well-established, the adaptation of pretrained 3D models for volumetric medical imaging remains underexplored. This work systematically investigates the effectiveness of video-pretrained models for AD classification, addressing questions about optimal architectural choices and transfer strategies.

- Methodological rigor: Many published studies suffer from methodological flaws
 including scan-level partitioning and improper validation protocols. This research
 implements rigorous subject-level validation methodology to provide realistic performance assessments for clinical applicability.
- 3. **Preprocessing optimization:** The impact of different preprocessing choices on transfer learning performance is incompletely understood. This work develops an optimized pipeline specifically designed to preserve diagnostically relevant features while standardizing inputs for deep learning models.
- 4. Architectural comparison: Limited research exists comparing architectures specifically optimized for video classification (r3d_18, MC3, R2Plus1D) on neuroimaging tasks. This study comprehensively evaluates these variants to determine the optimal approach for volumetric MRI analysis while maintaining computational feasibility.

These research gaps directly inform the methodology presented in the next section, which implements a rigorous experimental framework to evaluate video-pretrained model transfer for Alzheimer's disease detection. By addressing these gaps, this work aims to advance the field toward more accurate, reliable, and clinically applicaearch gaps and proposed solutions

4 Methodology

4.1 Data Acquisition and Characteristics

The Alzheimer's Disease Neuroimaging Initiative (ADNI) database served as the primary data source, providing standardized MRI acquisitions with corresponding clinical diagnoses. ADNI was selected over alternatives (including OASIS) for its comprehensive coverage, acquisition protocols, and expert-validated diagnoses [42, 43].

4.1.1 Dataset Composition

All selected scans were T1-weighted MPRAGE sequences (1.5T or 3T, 1mm³ isotropic resolution), chosen for optimal gray/white matter contrast, standardized acquisition parameters, and sensitivity to atrophy biomarkers. Additionally, the widespread clinical availability and established role of MPRAGE in AD assessment made it an ideal choice for this study. The final dataset contained 1,300 scans from 408 unique subjects, balanced between diagnostic categories:

Partition	AD	$\mathbf{C}\mathbf{N}$
Training	512 scans (133 subjects)	511 scans (115 subjects)
Validation	69 scans (35 subjects)	70 scans (45 subjects)
Test	69 scans (35 subjects)	69 scans (45 subjects)

Table 6: Distribution of scans and subjects across dataset partitions

4.1.2 Diagnostic Criteria

Subjects were classified as Alzheimer's Disease (AD) or Cognitively Normal (CN) based on NINCDS-ADRDA criteria. Initially, the dataset contained approximately 33% AD and 67% CN cases. To address class imbalance and potential overfitting issues identified during preliminary experiments, additional AD scans were incorporated and CN subjects carefully sampled to achieve a balanced 50/50 diagnostic distribution.

The binary classification focus (excluding Mild Cognitive Impairment) reflects the clearer structural changes observable in established AD, particularly hippocampal atrophy, which serves as a primary biomarker for disease progression. Subject-level isolation between dataset partitions was strictly enforced to prevent data leakage, ensuring realistic performance assessment for unseen individuals.

4.2 Preprocessing Pipeline

4.2.1 Initial Processing and Skull Stripping

Raw DICOM images were converted to NIfTI format using dicom2nifti with reorient-ation and compression enabled. This created unified volumetric files suitable for 3D analysis. Skull stripping was performed using SynthStrip, a deep learning-based method that represents the current state-of-the-art for brain extraction [35]. It was selected for its superior performance with atrophied brains. Unlike traditional threshold-based methods (e.g., BET), SynthStrip preserved critical cortical boundaries even with atrophied brains and better handled the variability in the ADNI dataset. Despite requiring 2.5 minutes per scan, the improved quality justified this approach by preventing potential misinterpretation of artifacts as disease-related changes.

4.2.2 Volume Standardization

All volumes were resampled to isotropic $1\times1\times1$ mm voxels using ANTs with third-order spline interpolation. This standardization ensured consistent spatial representation, eliminated scanner-specific resolution variability, and enabled uniform convolutional filter operations across all dimensions.

4.2.3 Adaptive Cropping Strategy

A key methodological innovation was the implementation of an adaptive cropping procedure followed by reshaping to $128 \times 128 \times 128$ dimensions. The approach:

- 1. Identified brain-containing regions using intensity thresholding
- 2. Applied cropping with minimal padding (3 voxels)
- 3. Used cubic interpolation to reach the target dimensions

This method preserved approximately 35% more effective resolution for critical structures like the hippocampus compared to naive downsampling. The 128³ dimension balanced preserving anatomical detail with memory constraints for model training.

4.2.4 Intensity Normalization and Orientation

N4 bias field correction was applied to mitigate intensity inhomogeneities from magnetic field variations. This prevents intensity variations that might be misinterpreted as structural changes. All volumes were reoriented to Right-Anterior-Superior (RAS) orientation to ensure consistent directionality, allowing the model to focus solely on relevant structural differences rather than arbitrary orientation variations.

4.2.5 Omission of Spatial Normalization

Despite its common use in neuroimaging pipelines, registration to standard space (e.g., MNI152) was deliberately omitted for several reasons:

- 1. Preservation of native atrophy patterns that could be distorted during normalization
- 2. Reliance on CNN translation invariance to identify structures without explicit alignment
- 3. Avoidance of interpolation artifacts that might smooth critical structural boundaries
- 4. Computational efficiency gains without compromising classification performance

Validation experiments confirmed that models trained on native-space data performed comparably to or better than those using normalized data, supporting this methodological decision and aligning with recent literature suggesting deep learning models for brain MRI benefit from native-space learning.

The entire pipeline produced 1,300 preprocessed volumes with consistent dimensions, orientation, and intensity characteristics while preserving the structural variations essential for AD classification.

4.3 Data Splitting Strategy

A methodologically rigorous data splitting approach was implemented to prevent data leakage while maintaining diagnostic balance across partitions. Unlike conventional image classification tasks, neuroimaging datasets require subject-level rather than scan-level splitting since multiple scans often exist for the same individual.

4.3.1 Subject-Level Isolation

A strict subject-level isolation approach ensured no individual appeared in multiple dataset partitions—a critical decision after initial experiments revealed artificially inflated performance metrics (90% accuracy) when subjects were allowed to cross partition boundaries. Complete subject isolation produced a more realistic performance assessment (77% accuracy), better reflecting the model's generalization capability to unseen individuals.

4.3.2 Partition Distribution

The dataset was divided following an 80/10/10 (train/validation/test) ratio using a round-robin algorithm that:

- 1. Grouped subjects by diagnostic condition
- 2. Sorted subjects in ascending order by scan count
- 3. Allocated subjects to partitions round robin to insure subject diversity across partitions
- 4. Final scan counts were balanced to maintain equal scan counts per diagnostic category

This approach yielded a balanced distribution with 1,023 training scans (512 AD/511 CN), 139 validation scans (69 AD/70 CN), and 138 test scans (69 AD/69 CN). The strict isolation maintained 203 unique subjects in training, 80 in validation, and 80 in test sets, with diagnostic balance preserved in each partition.

Data Leakage Prevention To prevent subtle forms of data leakage, subject identifiers were rigorously tracked and preprocessing parameters (such as intensity normalization statistics) were computed independently within each partition. This methodologically sound approach ensured that performance metrics would accurately reflect the model's ability to generalize to entirely new individuals, rather than merely recognizing previously seen subjects in different scans.

4.4 Data Augmentation

Data augmentation was strategically implemented to improve model generalization while preserving diagnostically relevant features. Through systematic experimentation, a minimal yet effective set of transformations was identified:

```
tio.Compose([
    tio.RandomNoise(mean=0.0, std=0.1, p=0.3),
    tio.RandomGamma(log_gamma=(-0.2, 0.2), p=0.3),
    tio.ZNormalization(),
])
```

This approach was applied exclusively to the training set, while validation and test sets received only Z-normalization to maintain evaluation consistency.

Each technique addressed specific neuroimaging considerations: Random noise (30% probability, σ =0.1) simulated scanner variability and promoted robustness to image quality differences; Gamma adjustment (\pm 0.2 range, 30% probability) mimicked contrast variations between scanners; Z-normalization standardized intensity values across all scans for consistent feature extraction.

Notably, several common augmentation techniques were deliberately excluded after experimental evaluation showed either no benefit or negative impact:

- Geometric transformations (rotations, flips) significantly increased training time (20 vs 5 epochs) without improving validation accuracy, likely due to inherent orientation variability already present in MRI data.
- Random scaling (0.9-1.1) showed no generalization improvement and potentially disrupted the carefully standardized voxel dimensions.

The final strategy evolved from extensive transformations to this focused set through iterative evaluation of validation performance and convergence speed, representing an optimal balance between enhancing robustness and preserving critical structural features essential for AD classification.

4.5 Model Architectures

4.5.1 3D ResNet Architecture

The primary model was a modified 3D ResNet-18 (r3d_18), selected for its residual connections that mitigate vanishing gradients, fully 3D convolutional operations to preserve volumetric spatial relationships, and parameter efficiency (33M parameters) enabling training on consumer hardware. The ResNet architecture family has demonstrated robust

performance across numerous computer vision tasks, including medical imaging applications, and is used frequently in the literature. The implementation used PyTorch's pre-trained r3d_18 model, with the first layer modified to accept single-channel MRI volumes and the final layer adapted for binary classification.

The model architecture consisted of 18 layers, with the first layer being a 3D convolutional layer followed by four residual blocks, each containing two 3D convolutional layers. The final fully connected layer was adapted to output binary classification scores. The model was trained using a transfer learning approach, leveraging pre-trained weights from the Kinetics 400 dataset, which provided a strong initialization for the feature extraction layers.

4.5.2 Transfer Learning Strategy

We implemented a selective transfer learning approach, freezing early convolutional layers (25% of parameters) while allowing the final residual block and fully connected layer (75%) to adapt to MRI-specific features. This balanced preserving pre-trained knowledge with domain adaptation. Initial experiments with more aggressive freezing (keeping only the final fully connected layer trainable) resulted in numerical instabilities during training, manifested as NaN losses, suggesting that significant domain adaptation was necessary given the substantial differences between video action recognition and MRI classification.

A differential learning rate strategy applied a $10 \times$ higher learning rate to the newly initialized fully connected layer compared to the fine-tuned convolutional layers, enabling aggressive adaptation in the task-specific output layer while making more conservative updates to the pre-trained feature extraction layers.

4.5.3 Architecture Comparison

To validate architectural choices, models were systematically evaluated with decreasing levels of 3D feature extraction:

1. **Mixed Convolution 3D Network**: This model (MC3-18) uses a hybrid approach combining 2D and 3D convolutions, hypothesized to potentially offer computational efficiency while maintaining performance.

Experimental results with MC3-18 showed less stable training dynamics and inferior performance compared to the pure 3D approach of R3D-18, supporting the importance of fully volumetric feature extraction for structural MRI analysis. The differences in performance provided empirical justification for the primary architectural choice.

2. (2+1)D Convolution Network: Following the investigation of MC3-18, a (2+1)D

architecture was also evaluated. This approach decomposes 3D convolutions into separate spatial (2D) and temporal (1D) convolutions, a technique that has shown promise in video classification tasks.

Results with the (2+1)D architecture revealed performance that was slightly worse than MC3-18, continuing the observed trend that classification accuracy decreased as the model architecture incorporated more 2D elements. This progression (R3D > MC3 > (2+1)D) strongly suggests that preserving the full 3D spatial context through pure 3D convolutions is critical for detecting the subtle volumetric patterns associated with Alzheimer's disease in MRI data.

- 3. Multiscale Vision Transformer: Recent advances in vision transformers prompted investigation of their potential for 3D MRI classification. However, initial implementation attempts revealed significant computational barriers:
 - (a) Memory requirements exceeded available hardware capabilities (32GB RAM requirement for 128×128×128 volumes)
 - (b) Architectural mismatch between the input dimensions required by MViT (designed for $16 \times 224 \times 224$ video clips) and the cubical $128 \times 128 \times 128$ MRI volumes
 - (c) Transformer architectures typically require substantially larger training datasets than were available

These constraints prevented full evaluation of transformer-based approaches, highlighting an important practical limitation in applying state-of-the-art vision models to medical imaging with limited computational resources.

4.5.4 Parameter Counts and Computational Considerations

The final model architecture parameters were:

• **Total parameters**: 33,148,482

• Trainable parameters: 24,909,826 (75.15%)

• Frozen parameters: 8,238,656 (24.85%)

These figures represent a significant reduction compared to larger architectures like ResNet-50 or ViT variants, making training feasible on consumer-grade hardware while maintaining sufficient capacity for the classification task. The reduced parameter count also potentially mitigated overfitting given the relatively small dataset size.

4.6 Training Framework and Implementation

Training was conducted on an M1 Mac using Metal Performance Shaders, with each epoch requiring approximately one hour and full training runs taking 20 hours. This hardware constrained batch size and architecture selection. Despite attempts at optimization through mixed precision training and CPU-GPU synchronization, computational bottlenecks in the model's forward pass remained.

Hyperparameters were selected through systematic experimentation and tracked with Weights & Biases:

Parameter	Value	Rationale	
Learning rate	0.001 (FC), 0.0001 (conv)	Differential rates for aggress-	
		ive output adaptation with	
		conservative updates to pre-	
		trained layers	
Optimizer AdamW (weight decay=0.01)		Effective regularization for the	
		limited dataset	
Batch size	2	Memory constraints from 128 ³	
		inputs	
LR schedule	Cosine annealing $(T_0=5)$	Prevents convergence to local	
		minima	

Table 7: Optimized hyperparameter configuration

A weighted cross-entropy loss function addressed potential class imbalance with weights dynamically calculated based on class distribution, particularly important during initial experiments when the dataset had not yet been fully balanced. This ensured balanced contribution to loss regardless of class representation.

Early stopping with patience=5 monitored both validation accuracy and loss, ensuring training continued as long as either metric showed enhancement, preventing overfitting while optimizing computational resources. Most models converged within 5-10 epochs, with early stopping typically triggering around epoch 7-8—quick convergence attributable to the transfer learning initialization.

A comprehensive checkpoint system saved regular epoch checkpoints and best models based on both accuracy and loss metrics. Each checkpoint stored model weights, optimizer state, scheduler state, and performance metrics for seamless training resumption. The system integrated with Weights & Biases to log best models as artifacts.

The training loop was implemented with careful attention to numerical stability and memory management. Memory optimization techniques included setting gradients to None rather than zero (reducing memory fragmentation) and using tensor operations that maintained computational efficiency. For MPS acceleration, explicit cache clearing was performed at the end of each epoch to prevent memory accumulation.

4.7 Evaluation Methodology

4.7.1 Performance Metrics

A comprehensive set of metrics was implemented to evaluate model performance beyond simple accuracy:

- Accuracy and balanced accuracy: The latter particularly important for medical applications as it equalizes the contribution of each diagnostic class.
- **Precision and recall**: Critical for clinical utility, measuring correct positive predictions and the ability to identify true AD cases, respectively.
- **Specificity**: Quantified the model's ability to correctly identify CN cases (TN/(TN+FP)).
- F1-score, ROC-AUC, and average precision: Provided threshold-independent performance assessment.

All metrics were continuously tracked and logged using a custom MetricsManager class, with implementation details provided in Appendix X.

4.7.2 Validation Strategy

The evaluation framework employed strict subject-level isolation to prevent data leakage:

- Dedicated validation (10%) and test (10%) sets maintained complete separation from training data.
- Multiple model checkpoints were saved (best accuracy and best loss) to mitigate selection bias.
- Final evaluation used only the held-out test set with the best validation accuracy checkpoint.

4.7.3 Statistical Analysis

Statistical rigor was ensured through:

- Bootstrap confidence intervals for key metrics to quantify the uncertainty in performance estimates
- Confusion matrix analysis to identify classification patterns
- Comparison to baselines: random chance (50%), clinical radiologist performance, and published algorithmic approaches

4.7.4 Cross-Validation and Architecture Evaluation

Despite computational constraints (20-hour training runs on M1 Mac), model robustness was verified through:

- Subject-level 3-fold cross-validation with diagnostic balance and subject-level isolation maintained across all partitions.
- Systematic architecture comparison across R3D-18, MC3-18, and R2Plus1D-18 to assess the impact of dimensional processing on performance and to validate the choice of fully 3D convolutional architectures
- Visualization techniques to provide qualitative insights into model behavior, rather than relying solely on quantitative metrics

Cross-validation reveal performance consistency across subject groupings, while architectural evaluation demonstrate whether fully 3D convolutional approaches systematically outperform partial 2D/3D hybrid methods

5 Results

6 Discussion

7 Conclusions

References

- [1] C. R. Jack, D. S. Knopman, W. J. Jagust, R. C. Petersen, M. W. Weiner, P. S. Aisen, L. M. Shaw, P. Vemuri, H. J. Wiste, S. D. Weigand et al., "Tracking pathophysiological processes in alzheimer's disease: an updated hypothetical model of dynamic biomarkers," The lancet neurology, vol. 12, no. 2, pp. 207–216, 2013.
- [2] P. Vemuri and C. R. Jack, "Role of structural mri in alzheimer's disease," *Alzheimer's research & therapy*, vol. 2, pp. 1–10, 2010.
- [3] C. R. Jack Jr, R. C. Petersen, P. C. O'brien, and E. G. Tangalos, "Mr-based hippocampal volumetry in the diagnosis of alzheimer's disease," *Neurology*, vol. 42, no. 1, pp. 183–183, 1992.
- [4] R. Cuingnet, E. Gerardin, J. Tessieras, G. Auzias, S. Lehéricy, M.-O. Habert, M. Chupin, H. Benali, O. Colliot, A. D. N. Initiative et al., "Automatic classification of patients with alzheimer's disease from structural mri: a comparison of ten methods using the adni database," neuroimage, vol. 56, no. 2, pp. 766–781, 2011.

- [5] L. Ferrarini, W. M. Palm, H. Olofsen, M. A. van Buchem, J. H. Reiber, and F. Admiraal-Behloul, "Shape differences of the brain ventricles in alzheimer's disease," *Neuroimage*, vol. 32, no. 3, pp. 1060–1069, 2006.
- [6] L. Gutiérrez-Galve, M. Lehmann, N. Z. Hobbs, M. J. Clarkson, G. R. Ridgway, S. Crutch, S. Ourselin, J. M. Schott, N. C. Fox, and J. Barnes, "Patterns of cortical thickness according to apoe genotype in alzheimer's disease," *Dementia and geriatric* cognitive disorders, vol. 28, no. 5, pp. 461–470, 2009.
- [7] B. Dubois, H. H. Feldman, C. Jacova, S. T. DeKosky, P. Barberger-Gateau, J. Cummings, A. Delacourte, D. Galasko, S. Gauthier, G. Jicha et al., "Research criteria for the diagnosis of alzheimer's disease: revising the nincds-adrda criteria," The Lancet Neurology, vol. 6, no. 8, pp. 734–746, 2007.
- [8] C. R. Jack Jr, D. A. Bennett, K. Blennow, M. C. Carrillo, B. Dunn, S. B. Haeberlein, D. M. Holtzman, W. Jagust, F. Jessen, J. Karlawish *et al.*, "Nia-aa research framework: toward a biological definition of alzheimer's disease," *Alzheimer's & dementia*, vol. 14, no. 4, pp. 535–562, 2018.
- [9] S. Klöppel, C. M. Stonnington, J. Barnes, F. Chen, C. Chu, C. D. Good, I. Mader, L. A. Mitchell, A. C. Patel, C. C. Roberts et al., "Accuracy of dementia diagnosis—a direct comparison between radiologists and a computerized method," Brain, vol. 131, no. 11, pp. 2969–2974, 2008.
- [10] L. J. Herrera, I. Rojas, H. Pomares, A. Guillén, O. Valenzuela, and O. Baños, "Classification of mri images for alzheimer's disease detection," in 2013 international conference on social computing. IEEE, 2013, pp. 846–851.
- [11] G. Litjens, T. Kooi, B. E. Bejnordi, A. A. A. Setio, F. Ciompi, M. Ghafoorian, J. A. Van Der Laak, B. Van Ginneken, and C. I. Sánchez, "A survey on deep learning in medical image analysis," *Medical image analysis*, vol. 42, pp. 60–88, 2017.
- [12] G. Liang, X. Xing, L. Liu, Y. Zhang, Q. Ying, A.-L. Lin, and N. Jacobs, "Alzheimer's disease classification using 2d convolutional neural networks," in 2021 43rd annual international conference of the ieee engineering in medicine & biology society (embc). IEEE, 2021, pp. 3008–3012.
- [13] S. Sarraf and G. Tofighi, "Classification of alzheimer's disease structural mri data by deep learning convolutional neural networks," arXiv preprint arXiv:1607.06583, 2016.
- [14] K. Gunawardena, R. Rajapakse, and N. D. Kodikara, "Applying convolutional neural networks for pre-detection of alzheimer's disease from structural mri data," in

- 2017 24th international conference on mechatronics and machine vision in practice (M2VIP). IEEE, 2017, pp. 1–7.
- [15] A. Payan and G. Montana, "Predicting alzheimer's disease: a neuroimaging study with 3d convolutional neural networks," arXiv preprint arXiv:1502.02506, 2015.
- [16] J. Yang, X. Huang, Y. He, J. Xu, C. Yang, G. Xu, and B. Ni, "Reinventing 2d convolutions for 3d images," *IEEE Journal of Biomedical and Health Informatics*, vol. 25, no. 8, pp. 3009–3018, 2021.
- [17] M. Hon and N. M. Khan, "Towards alzheimer's disease classification through transfer learning," in 2017 IEEE International conference on bioinformatics and biomedicine (BIBM). IEEE, 2017, pp. 1166–1169.
- [18] A. Ebrahimi-Ghahnavieh, S. Luo, and R. Chiong, "Transfer learning for alzheimer's disease detection on mri images," in 2019 IEEE international conference on industry 4.0, Artificial intelligence, and communications technology (IAICT). IEEE, 2019, pp. 133–138.
- [19] A. Mehmood, S. Yang, Z. Feng, M. Wang, A. S. Ahmad, R. Khan, M. Maqsood, and M. Yaqub, "A transfer learning approach for early diagnosis of alzheimer's disease on mri images," *Neuroscience*, vol. 460, pp. 43–52, 2021.
- [20] M. Maqsood, F. Nazir, U. Khan, F. Aadil, H. Jamal, I. Mehmood, and O.-y. Song, "Transfer learning assisted classification and detection of alzheimer's disease stages using 3d mri scans," Sensors, vol. 19, no. 11, p. 2645, 2019.
- [21] Q. Yang, N. Li, Z. Zhao, X. Fan, E. I.-C. Chang, and Y. Xu, "Mri cross-modality image-to-image translation," *Scientific reports*, vol. 10, no. 1, p. 3753, 2020.
- [22] J. P. Kieselmann, C. D. Fuller, O. J. Gurney-Champion, and U. Oelfke, "Cross-modality deep learning: contouring of mri data from annotated ct data only," *Medical physics*, vol. 48, no. 4, pp. 1673–1684, 2021.
- [23] H. Wu, J. Luo, X. Lu, and Y. Zeng, "3d transfer learning network for classification of alzheimer's disease with mri," *International Journal of Machine Learning and Cybernetics*, vol. 13, no. 7, pp. 1997–2011, 2022.
- [24] Y. Tang, D. Yang, W. Li, H. R. Roth, B. Landman, D. Xu, V. Nath, and A. Hatamiz-adeh, "Self-supervised pre-training of swin transformers for 3d medical image analysis," in *Proceedings of the IEEE/CVF conference on computer vision and pattern recognition*, 2022, pp. 20730–20740.

- [25] A. Ebrahimi, S. Luo, and R. Chiong, "Introducing transfer learning to 3d resnet-18 for alzheimer's disease detection on mri images," in 2020 35th international conference on image and vision computing New Zealand (IVCNZ). IEEE, 2020, pp. 1–6.
- [26] H. Acharya, R. Mehta, and D. K. Singh, "Alzheimer disease classification using transfer learning," in 2021 5th International Conference on Computing Methodologies and Communication (ICCMC). IEEE, 2021, pp. 1503–1508.
- [27] C. Davatzikos, "Machine learning in neuroimaging: Progress and challenges," pp. 652–656, 2019.
- [28] D. Tran, H. Wang, L. Torresani, J. Ray, Y. LeCun, and M. Paluri, "A closer look at spatiotemporal convolutions for action recognition," in *Proceedings of the IEEE conference on Computer Vision and Pattern Recognition*, 2018, pp. 6450–6459.
- [29] Y. Lyu, X. Yu, D. Zhu, and L. Zhang, "Classification of alzheimer's disease via vision transformer: Classification of alzheimer's disease via vision transformer," in *Proceedings of the 15th international conference on PErvasive technologies related to assistive environments*, 2022, pp. 463–468.
- [30] H. Yan, V. Mubonanyikuzo, T. E. Komolafe, L. Zhou, T. Wu, and N. Wang, "Hybrid-rvit: Hybridizing resnet-50 and vision transformer for enhanced alzheimer's disease detection," *PloS one*, vol. 20, no. 2, p. e0318998, 2025.
- [31] S.-Y. Lu, Y.-D. Zhang, and Y.-D. Yao, "An efficient vision transformer for alzheimer's disease classification using magnetic resonance images," *Biomedical Signal Processing* and Control, vol. 101, p. 107263, 2025.
- [32] S. Basaia, F. Agosta, L. Wagner, E. Canu, G. Magnani, R. Santangelo, M. Filippi, A. D. N. Initiative et al., "Automated classification of alzheimer's disease and mild cognitive impairment using a single mri and deep neural networks," NeuroImage: Clinical, vol. 21, p. 101645, 2019.
- [33] N. Garg, M. S. Choudhry, and R. M. Bodade, "A review on alzheimer's disease classification from normal controls and mild cognitive impairment using structural mr images," *Journal of neuroscience methods*, vol. 384, p. 109745, 2023.
- [34] A. Fatima, A. R. Shahid, B. Raza, T. M. Madni, and U. I. Janjua, "State-of-the-art traditional to the machine-and deep-learning-based skull stripping techniques, models, and algorithms," *Journal of Digital Imaging*, vol. 33, pp. 1443–1464, 2020.
- [35] A. Hoopes, J. S. Mora, A. V. Dalca, B. Fischl, and M. Hoffmann, "Synthstrip: skull-stripping for any brain image," *NeuroImage*, vol. 260, p. 119474, 2022.

- [36] V. Viswan, F. Hajamohideen, K. Subramanian, N. Shaffi, and M. Mahmud, "Enhancing insights: unravelling the potential of preprocessing mri for artificial intelligence based alzheimer's disease classification," *Machine Learning Models and Architectures for Biomedical Signal Processing*, pp. 125–151, 2025.
- [37] A. Farooq, S. Anwar, M. Awais, and S. Rehman, "A deep cnn based multi-class classification of alzheimer's disease using mri," in 2017 IEEE International Conference on Imaging systems and techniques (IST). IEEE, 2017, pp. 1–6.
- [38] P. Saikia and S. K. Kalita, "Alzheimer disease detection using mri: deep learning review," *SN Computer Science*, vol. 5, no. 5, p. 507, 2024.
- [39] V. Mubonanyikuzo, H. Yan, T. E. Komolafe, L. Zhou, T. Wu, and N. Wang, "Detection of alzheimer disease in neuroimages using vision transformers: Systematic review and meta-analysis," *Journal of Medical Internet Research*, vol. 27, p. e62647, 2025.
- [40] M. Menagadevi, S. Devaraj, N. Madian, and D. Thiyagarajan, "Machine and deep learning approaches for alzheimer disease detection using magnetic resonance images: An updated review," *Measurement*, vol. 226, p. 114100, 2024.
- [41] N. Pradhan, S. Sagar, and A. S. Singh, "Analysis of mri image data for alzheimer disease detection using deep learning techniques," *Multimedia Tools and Applications*, vol. 83, no. 6, pp. 17729–17752, 2024.
- [42] C. R. Jack Jr, M. A. Bernstein, N. C. Fox, P. Thompson, G. Alexander, D. Harvey, B. Borowski, P. J. Britson, J. L. Whitwell, C. Ward et al., "The alzheimer's disease neuroimaging initiative (adni): Mri methods," Journal of Magnetic Resonance Imaging: An Official Journal of the International Society for Magnetic Resonance in Medicine, vol. 27, no. 4, pp. 685–691, 2008.
- [43] P. J. LaMontagne, T. L. Benzinger, J. C. Morris, S. Keefe, R. Hornbeck, C. Xiong, E. Grant, J. Hassenstab, K. Moulder, A. G. Vlassenko et al., "Oasis-3: longitudinal neuroimaging, clinical, and cognitive dataset for normal aging and alzheimer disease," medrxiv, pp. 2019–12, 2019.